RSS Tech. Rpt. 04262021 April 26, 2021

Technical Report: Remote Sensing Systems

A Diurnal Warming Model for the Sub-Skin Temperature of the Ocean

Frank J. Wentz
Katherine Wentz
Richard Lindsley

Prepared By

Remote Sensing Systems
444 Tenth Street, Suite 200, Santa Rosa, CA 95401 (707) 545-2904

Table of Contents

1 Introduction

1.1 Importance of Sea Surface Temperature in Climate Studies

Sea surface temperature (SST) is a fundamental variable at the air-sea interface that drives and interacts with the coupled ocean-atmosphere system. SST is classified as an Essential Climate Variable by the Global Climate Observing System (GCOS 2015). Oceanographers, meteorologists, and climate scientists benefit from accurate SST maps. Moreover, SST measurements are used to observe and model changes in the global climate system, such as decadal climate patterns like the El Niño Southern Oscillation (ENSO), Western Pacific Warm Pool, and Madden-Julian Oscillation (MJO) (Kawai & Wada 2007). SST constitutes 71% of the surface area input into merged global land-ocean surface temperature data products, which are used in atmospheric general circulation models to calculate heat fluxes between the atmosphere and ocean. Recently SSTs have been used as climate model "pacemakers". For example, Kosaka and Xie (2013) used observed SSTs over the central-to-eastern tropical Pacific to train a climate model and, as a result, the model reproduced both global and regional temperatures and precipitation to a high degree of accuracy (r=0.97). In addition, SST is used in Numerical Weather Prediction (NWP) models to forecast ocean events such as hurricane trajectories (NCAR 2014). Beyond climate research and NWP seasonal monitoring, SST observations are useful for predicting coral bleaching, tracking pollution, and managing tourism and commercial fishery industries (NOAA 2020).

1.2 Satellite Measurements of SST Diurnal Warming

SST measurements may be collected in situ by buoys, which measure the water temperature at a depth of about 1 m. However, these point measurements can be too sparse for many applications, so satellites capable of providing near-global ocean coverage are additionally employed. For the purposes of retrieving SST from space, two complementary types of satellite sensors are used: microwave radiometers operating in the C and X bands (~7 to 10 GHz) and infrared radiometers operating in the mid- and long-wavelength bands (~3 to 12 μm). While the two classes of radiometers operate on similar physical principles of black-body radiation that relate the received power to physical temperature, the effective depth of the SST that they measure differs. Microwave sensors are sensitive to the SST at a sub-skin depth on the order of 1-2 mm whereas infrared sensors are sensitive to the SST at a skin depth on the order of 20 μm.

The temperature of the skin and sub-skin can have a significant diurnal warming, which is defined herein as the skin or sub-skin SST minus the foundation SST (1 – 5 m depth), where the water column is free of diurnal temperature variability. High solar insolation and low winds can increase the diurnal warming up to 5 C (Kawai & Wada 2007). Generally, diurnal warming peaks from prenoon to the late afternoon depending on the region (Stuart-Menteth et al. 2003).

Observations and models of diurnal warming are essential to the study of the diurnal exchange of heat between the atmosphere and the sea. For example, a large diurnal SST rise can lead to an increase in net surface heat flux from the ocean of 50-60 W/m^2 in the daytime. In addition, the solubility of gases like CO_2 and O_2 depend on the SST, and therefore fluctuate as a function of diurnal warming. Finally, diurnal warming at the ocean surface must be accurately modeled in order to reproduce SST variations on an intra-seasonal scale, and to understand biological and material circulation processes as a result of mixed-layer deepening or shoaling (Kawai & Wada 2007).

1.3 Diurnal Warming Models for Inter-Calibration of Satellite SST Measurements

Another important aspect of diurnal warming is its impact on the inter-calibration of satellite SST sensors. Satellites take observations at different local times. When merging satellite SST measurements into a consistent long-term climate record, it is essential to remove the diurnal warming component. By doing this, the long-term SST response to climate change is disentangled from the diurnal warming signal. Thus, any detailed analysis of satellite SST measurements must account for diurnal warming.

The physical processes governing diurnal warming are complex. The Goddard Earth Observing System (GEOS) AGCM SST model, for example, incorporates both above-ocean geophysical processes, i.e. net longwave and shortwave radiation, and sensible and latent heat fluxes, and below-ocean geophysical processes, i.e. molecular and turbulent mixing (Takaya et al. 2010). Other examples of diurnal warming models based on below-ocean diffusion and bulk energy transfer are given in Kawai & Wada (2007).

For the purpose of satellite inter-calibration, we need a simpler, more practical method for estimating the diurnal warming observed by the large array of satellite sensors. Our first diurnal warming model for doing this was empirical (Gentemann, Wentz, et al. 2003). The variation of the diurnal warming over the day was empirically derived by fitting a 10^{th} order Fourier expansion to satellite observations, thereby making the model totally dependent on the veracity of the satellite measurements. At that time, the only available satellite sensor for doing this type of analysis was the TRMM microwave imager (TMI). Unfortunately, TMI had an emissive antenna, and the effects related to the warming and cooling of the TMI antenna had to be removed from the observed SST diurnal variations. This inevitably introduced some error into the analysis. Furthermore, the 2003 model did not account for variations in the time of sunrise and the length of day, which are significant factors at higher latitudes.

In view of these deficiencies in the 2003 model and the availability of new, extremely high-quality satellite SST measurements from the GPM microwave imager (GMI), we decided to update the model. The new model is physically based, and the only terms that require training are the cooling time constant τ and the depth D of the diurnal layer.

2 A Simple, Physically-Based Diurnal Warming Model

2.1 Differential Equation for the Heating and Cooling of the Diurnal Layer

Herein we define diurnal warming, which is denoted by T, as the difference of the sub-skin temperature minus the foundation temperature. The diurnal warming model is represented by the following first-order linear differential equation in which the first term represents the heating the diurnal layer due to incoming solar radiation and the second term accounts for the cooling of the layer

$$\frac{\partial T}{\partial t} = \frac{F(t)}{D\rho C_p} - \frac{T}{\tau} \tag{1}$$

where t denotes time (hour) (equation 1). For the heating term, D (m) is the depth of the layer being heated, ρ (kg/m^3) is the density of water, C_p is the specific heat capacity (J/(kg·K)) of water, and F (J/(hour·m^2)) is the solar flux at the surface. For the cooling term, we assume the Newton's

cooling law for which the decrease in temperature is proportional to the difference of the layer temperature minus the temperature of the surrounding environment. In our case the temperature difference is the diurnal warming T. The term τ is the time constant of the system that determines the rate of cooling.

We acknowledge equation (1) is an over simplification of the flux processes occurring at the upper and lower boundaries of the diurnal layer. However, on average, the verification of the model against satellite SST measurements indicates the model performs surprising well given its simplicity. The limitations of the model are discussed in Section 2.8.

Equation (1) is a standard first-order linear differential equation with the following solution

$$T(t) = \frac{1}{D\rho C_p} \int_0^t e^{-\left(\frac{t-t'}{\tau}\right)} F(t')\, dt' \tag{2}$$

where we have used the boundary condition $T(0) = 0$ (equation 2). As we will discuss, the time constant τ varies from is 2.75 to 3.85 hours, and integrating back in time 12 hours is sufficient. So, in practice equation (2) is replaced by equation (3).

$$T(t) = \frac{1}{D\rho C_p} \int_{t-12}^t e^{-\left(\frac{t-t'}{\tau}\right)} F(t')\, dt' \tag{3}$$

2.2 Solar Flux at the Ocean Surface

The solar flux at the ocean surface is modeled by equation (4)

$$F(t) = 3600 \alpha G_{sc} \frac{r_{sun0}^2}{r_{sun}^2} \cos\Theta \tag{4}$$

where the leading factor 3600 converts flux from J/(sec·m^2) to J/(hour·m^2), which is required because (3) is in terms of t = hours. G_{sc} is the solar constant, r_{sun0} is the mean distance of the Earth from the sun, and r_{sun} is the distance at the observation time. The term α accounts for the reduction of the incoming solar flux due to the atmosphere. The time dependence in equation (4) is due to the solar zenith angle Θ varying over the course of a day. The solar zenith angle is given by equation (5)

$$\cos\Theta = \sin\Phi \sin\delta + \cos\Phi \cos\delta \cos\left(\beta_{sun} - \beta\right) \tag{5}$$

where Φ and β are the Earth latitude and longitude, and Φ_{sun} and β_{sun} are the sun latitude (i.e., declination) and longitude. The difference β_{sun} - β is the solar hour angle. The absorption and scattering by the atmosphere are modeled by equation (6)

$$\alpha = \left(1 - \alpha_{cloud}\right) e^{-\alpha_{gas} \sec\Theta} \tag{6}$$

where α_{cloud} = 0.25 and α_{gas} = 0.2. This expression assumes clouds scatter 25% of the incoming radiation back into space, and the exponential term assumes atmospheric gases absorb 18% of the incoming radiation at local noon (Θ = 0) (Lindsey 2009). The absorption term increases as the slant path of the incoming radiations increases in early morning and evening. The increase in the slant path follows the secant of the zenith angle. Averaged over the day, the atmospheric absorption is 25%.

The 25% reduction due to clouds is an average global amount and can vary considerably. This represents a significant limitation in applying the diurnal warming model to a particular location and time as opposed to using it for average conditions, such a monthly averages over a large area.

2.3 Depth of Diurnal Layer

The roughening of the ocean surface by wind has a major impact on the diurnal warming. We model the wind effect by having the depth of the diurnal layer, i.e. the mass of water that experiences warming, increase with increasing wind. This increase in depth is due to the increased mixing in the ocean boundary layer. To derive the relationship between the layer depth D (m) and wind speed W (m/s), we use GMI measurements of SST, as is discussed in Section 2.5. This relationship is shown below by equation (7)

$$D = D_0 e^{\mu W} \tag{7}$$

where $D_0 = 0.5$ m is the depth of the diurnal layer for zero wind speed, and $\mu = 0.46$ s/m. The wind speed is referenced to an anemometer height of 10 m. The depth increases exponentially with W, and above 7 m/s, the model predicts very little diurnal warming.

2.4 Cooling Time Constant

During the day, we find a cooling time constant of $\tau = 2.75$ hours provided a good fit to the GMI measurements of $T(t)$. However, later at night we find the cooling rate to be slower, presumably due to the colder environment, and using a somewhat large value for τ gives a better fit to the GMI observations. Accordingly, we use the following expression for τ

$$\begin{aligned} &\tau = 2.75 \quad 7 \geq t_{local} \geq 19 \\ &else \\ &\tau = 2.75 + 1.1 \cos d^2 \left[15 \left(t_{local} - 1 \right) \right] \end{aligned} \tag{8}$$

where t_{local} (hours) is local time of day (equation 8). Figure 1 shows the variation of τ through the day.

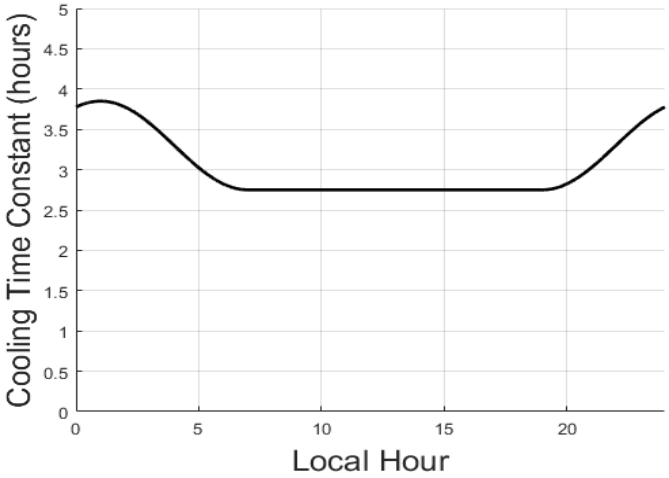

Fig. 1. Cooling Time Constant τ variation over the day.

2.5 Training the Diurnal Model Using GMI SST Measurements

The two elements of the model that require training are the depth of the diurnal layer D and the cooling time constant τ. The coefficients for these two parameters, i.e., equations (7) and (8), are adjusted so as to best match the model $T(t)$ to the diurnal warming measured by NASA's Global Precipitation Measurement Mission (GPM) Microwave Imager (GMI).

GMI was launched in 2014 and is now playing a vital role in microwave satellite retrievals. GMI has proven to be the most accurate microwave imager ever put into space due to its onboard dual calibration system, a flawless antenna, a well-designed hot load, and many other enhanced features. By virtue of GMI's advanced calibration system and a series of carefully planned GPM orbital maneuvers, GMI measures Earth's microwave emission with an RMS absolute accuracy of 0.25 K, as compared to the 1 - 2 K accuracy of previous sensors (Wentz & Draper 2016). GMI is ideal for measuring diurnal warming. It flies in a 65° inclined orbit and observes the complete 24-hour diurnal cycle over a period of about 80 days.

The computation of diurnal warming from the GMI measurements requires the specification of a foundation temperature. For the foundation SST, we used the National Climatic Data Center Daily Optimal Interpolation SSTs (commonly referred to as "Reynolds SST") and the Canadian Meteorological Centre (CMC) SST (Huang et al. 2021; CMC 2016). Both of these products are daily averages and represent the SST at depth. We performed separate analyses, one using Reynolds and the other using CMC. The results were remarkably close, and we decided to simply take the average of the two. The diurnal warming is then computed from equation (9).

$$T = SST_{1mm,GMI} - SST_{atdepth,rey,cmc} \tag{9}$$

The degree to which Reynolds and CMC actually represent the foundation temperature is somewhat uncertain. We found that the GMI 1-mm SST observations just before local sunrise closely corresponded to the Reynolds and CMC daily averages. We adjusted the Reynolds and CMC SSTs to exactly agree with these GMI pre-dawn observations. This adjustment consists of subtracting 0.08 C from Reynolds and 0.06 C from CMC. With this adjustment, our diurnal model is normalized so as to give T=0 near sunrise.

2.6 List of Model Parameters, Required Inputs, and Output

The tables in this section provide a list of the model parameters, the required inputs for the model, and the one output *T*.

Table 1: Parameters in diurnal warming model.

Parameter	Definition	Value	Units
ρ	Water Density	998	kg/m^2
C_p	Heat Capacity	4185.5	J/(kg C)
G_{sc}	Solar Constant	1361	W/m^2
r_{sun0}	Average Distance Between Earth and Sun	$149.6 * 10^6$	km
α_{cloud}	Fraction of Radiation Backscattered by Clouds	0.25	none
α_{gas}	Atmospheric Absorption Coefficient	0.2	none
D_0	Depth of Warming Layer for Zero Wind	0.5	m
μ	Wind Dependence Coefficient	0.46	s/m
τ	Cooling Time Constant	2.75 – 3.85	hours

Table 2: Inputs to Diurnal Warming Model

Variable Name	Definition	Units
Φ_{sun}	Sun Latitude (i.e., Declination)	degrees
β_{sun}	Sun Longitude	degrees
r_{sun}	Distance Between Earth and Sun	km
t	GMT Time of Day for Observation	hours
Φ	Earth Latitude	degrees
β	Earth East Longitude	degrees
W	Wind Speed Measured 10 m Above Surface	m/s

Table 3: Output from Diurnal Warming Model

Variable Name	Definition	Units
T	Diurnal Warming of Sub-Skin Layer	C

3 Model Performance Results

Four microwave sensors are used to evaluate the performance of the diurnal model: GMI, TMI, WindSat and AMSR2. The website www.remss.com provides detailed information on these sensors. All four sensors are capable of measuring SST. For each sensor we compute $T(t)$ from equation (9). These T values are averaged into 48 local time bins (i.e., every half hour) and 4 wind speed bins: 0 – 2.5 m/s, 2.5 – 4.5 m/s, 4.5 – 7.5 m/s, and 7.5 – 15.5 m/s. In addition to SST, each sensor is capable of measuring wind speed, and these wind measurements are used for the binning. GMI and TMI are in inclined orbits and observe the full diurnal cycle of the Earth. WindSat and AMSR2 are in fixed polar orbits and observe the Earth at fixed local times. For WindSat the local observation times are approximately 6 am and 6 pm, depending on latitude. For AMSR2 the times are 1:30 am and 1:30 pm.

Figure 2 shows the results. The GMI measurements of $T(t)$ agree well with the model, which is expected to some degree because GMI was used for training. There is also good model agreement with the other 3 sensors, which were withheld for training. More detailed results (not shown), for which the data are stratified according to latitude and season of year, show good performance over long summer days and short winter days.

4 Limitations and Future Improvements

One major limitation of the current model is that we are using a fixed number ($\alpha_{cloud} = 0.25$) for the backscattering of solar radiations by clouds. On clear days, the diurnal warming will be 25% higher and on very cloudy days it can be 25% or more less. This ±25% variation in $T(t)$ averages out when doing the large averages presented in Section 3. However, a major improvement would be to treat α_{cloud} as an ancillary input. The satellite microwave radiometers do measure total cloud water, but not cloud type. We plan to investigate if using the total cloud water measurement taken by the satellite as a proxy for α_{cloud} improves the performance of the model.

Likewise, the model does not account for precipitation. Precipitation will cause turbulent mixing of the upper layer and diminish diurnal warming in similar fashion as high winds. The satellite microwave radiometers also measure surface rain rate, and the feasibility of adding this information into the model is being investigated.

As we have acknowledged, equation (1) is an over simplification of the flux processes occurring at the upper and lower boundaries of the diurnal layer, such as the diurnal variation of skin cooling. Kawai & Wada (2007) suggest skin cooling is approximately the same between day and night. However, Alappattu et al. (2017) indicated that along the North Carolina coast, skin cooling increases in the late evening and decreases in the mid-afternoon. We are exploring the possibility of explicitly including the skin cooling effect in future iterations of the diurnal warming model. Our current investigation of comparing diurnal warming between microwave sensors (GMI, WindSat, AMSR2) and infrared sensors (VIIRS), both of which are collocated with the buoy at-depth SST measurements, may shed some light on this question given the two depths of the satellite measurements: 1-2 mm versus 20 μm.

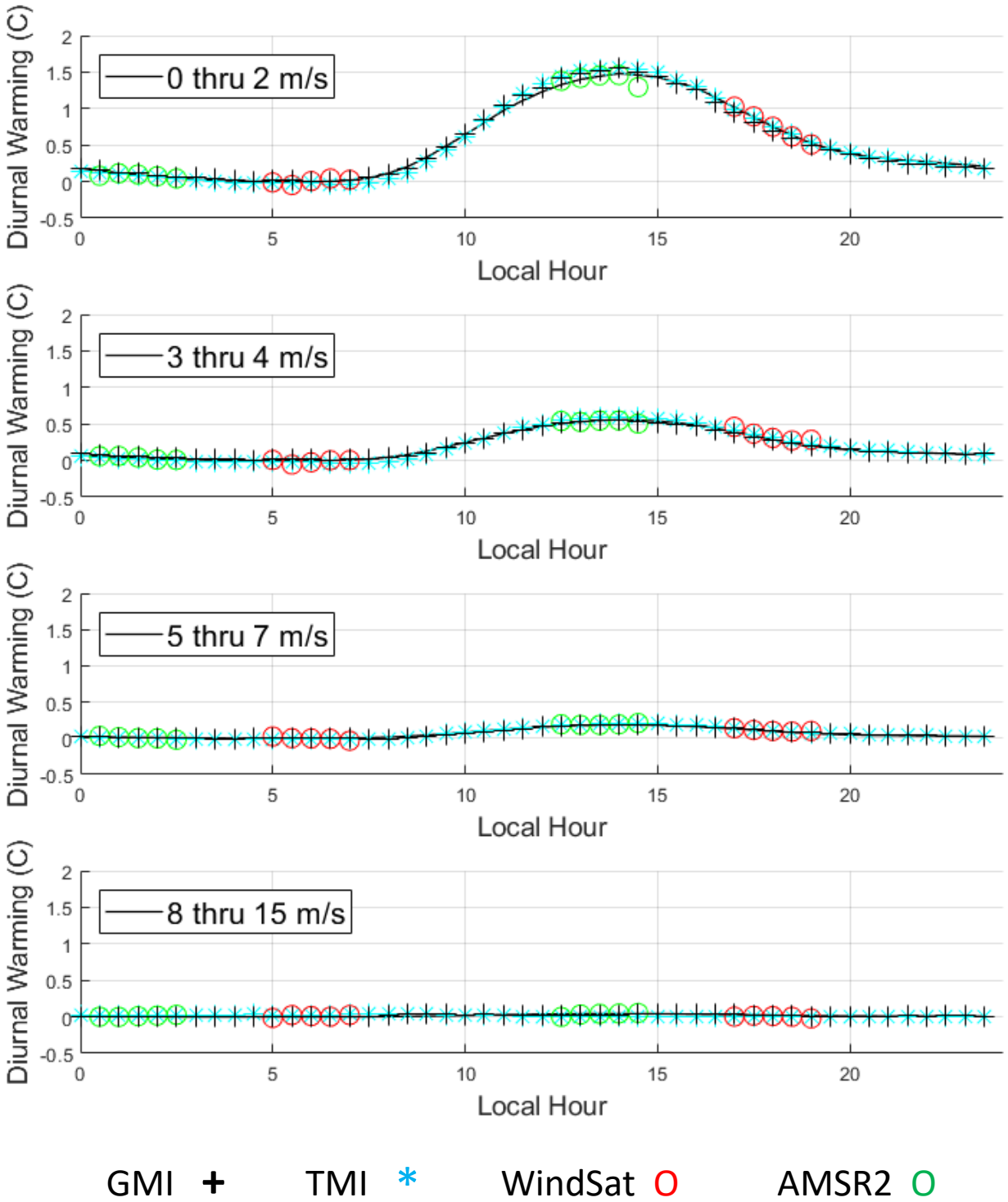

Fig. 2. Performance of diurnal warming model (black line). Each frame shows a different wind speed range. The GMI results, which were used for training, are shown by the black plus symbol. TMI, WindSat, and AMSR2, which were withheld from the training, are shown by the cyan asterisks, red circles, and green circles, respectively.

5 References

Alappattu, D.P., Q. Wang, R. Yamaguchi, R.J. Lind, M. Reynolds, A.J. Christman. 2017. Warm Layer and Cool Skin Corrections for Bulk Water Temperature Measurements for Air-Sea Interaction Studies. Journal of Geophysical Research: Oceans. 122(8), pp. 6470-6481. https://doi.org/10.1002/2017JC012688.

Canada Meteorological Center (CMC). 2016. CMC 0.1 deg global sea surface temperature analysis. Ver. 3.0. PO.DAAC, CA, USA. https://doi.org/10.5067/GHCMC-4FM03.

Global Climate Observing System (GCOS)-195. 2015. Status of the Global Observing System for Climate, [Stephen Briggs, Chairperson of the GCOS Steering Committee]. Global Climate Observing System, World Meteorological Organization (WMO). Geneva, Switzerland. 353.

Gentemann C.L., C.J. Donlon, A. Stuart-Menteth, & F.J. Wentz. 2003. Diurnal Signals in Satellite Sea Surface Temperature Measurements. Geophysical Research Letters. 30(3). https://doi.org/10.1029/2002GL016291.

Huang, B., C. Liu, V. Banzon, E. Freeman, G. Graham, W. Hankins, T. Smith, and H.-M. Zhang, 2021: Improvements of the Daily Optimum Sea Surface Temperature (DOISST) - Version 2.1, Journal of Climate. 34, pp. 2923-2939. https://doi.org/10.1175/JCLI-D-20-0166.1.

Kawai, Y. and A. Wada. 2007. Diurnal Sea Surface Temperature Variation and Its Impact on the Atmosphere and Ocean: A Review. Journal of Oceanography. 63, pp. 721-744. http://dx.doi.org/10.1007/s10872-007-0063-0.

Kosaka, Y. & S. Xie. 2013. Recent Global-Warming Hiatus Tied to Equatorial Pacific Surface Cooling. Nature Letter. 501. https://doi.org/10.1038/nature12534.

Lindsey, R. 2009. Climate and Earth's Energy Budget. NASA Earth Observatory Article. https://earthobservatory.nasa.gov/features/EnergyBalance. 04/26/21.

National Center for Atmospheric Research (NCAR). 2014. The Climate Data Guide: SST Data Sets: Overview & Comparison Table. https://climatedataguide.ucar.edu/climate-data/sst-data-sets-overview-comparison-table

National Oceanic and Atmospheric Administration (NOAA). 2020. Why do scientists measure sea surface temperature? National Ocean Service Website. https://oceanservice.noaa.gov/facts/sea-surface-temperature.html, 12/04/20.

Stuart-Menteth, A.C., I.S. Robinson, P.G. Challenor. 2003. A Global Study of Diurnal Warming Using Satellite-Derived Sea Surface Temperature. Journal of Geophysical Research. 108(C5). https://doi.org/10.1029/2002JC001534.

Takaya, Y., J. Bidlot, A.C. Beljaars, P.A. Janssen. 2010. Refinements to a Prognostic Scheme of Skin Sea Surface Temperature. Journal of Geophysical Research: Oceans. 115(C6). https://doi.org/10.1029/2009JC005985.

Wentz, F. & D. Draper. 2016. On-Orbit Absolute Calibration of the Global Precipitation Measurement Microwave Imager. Journal of Atmospheric and Oceanic Technology. 33(7), pp. 1393-1412. https://doi.org/10.1175/JTECH-D-15-0212.1.